AGU ADVANCING EARTH AND SPACE SCIENCES

Earth and Space Science

RESEARCH ARTICLE
10.1029/2024EA003852

Special Collection:
Surface Topography and Vegetation: Science, Measurements, and Technologies

InSAR Observations of Construction-Induced Coastal Subsidence on Miami's Barrier Islands, Florida

Farzaneh Aziz Zanjani[1], Falk Amelung[1], Andreas Piter[2], Khaled Sobhan[3], Amin Tavakkoliestahbanati[4], Gregor P. Eberli[1], Mahmud Haghshenas Haghighi[2], Mahdi Motagh[2,5], Pietro Milillo[4,6], Sara Mirzaee[7], Antonio Nanni[8], and Esber Andiroglu[8]

[1]Deparment of Marine Geoscience, Rosenstiel School of Marine and Atmospheric and Earth Science, University of Miami, Miami, FL, USA, [2]Leibniz University Hannover, Institute of Photogrammetry and Geoinformation, Hannover, Germany, [3]Department of Civil, Environmental, and Geomatics Engineering, Florida Atlantic University, Boca Raton, FL, USA, [4]Department of Civil and Environmental Engineering, University of Houston, Houston, TX, USA, [5]Department of Geodesy, GFZ German Research Centre for Geosciences, Potsdam, Germany, [6]German Aerospace Center (DLR), Microwaves and Radar Institute, Munich, Germany, [7]California Institute of Technology (Caltech), Pasadena, CA, USA, [8]Department of Civil and Architectural Engineering, College of Engineering, University of Miami, Miami, FL, USA

Abstract This study utilizes Interferometric Synthetic Aperture Radar (InSAR) to examine subsidence along the coastal strip of the Miami barrier islands from 2016 to 2023. Using Sentinel-1 data, we document vertical displacements ranging from 2 to 8 cm, affecting a total of 35 coastal buildings and their vicinity. About half of the subsiding structures are younger than 2014 and at the majority of them subsidence decays with time. This correlation suggests that the subsidence is related to construction activities. In northern and central Sunny Isles Beach, where 23% of coastal structures were built during the last decade, nearly 70% are experiencing subsidence. The majority of the older subsiding structures show sudden onset or sudden acceleration of subsidence, suggesting that this is due to construction activities in their vicinity; we have identified subsidence at distance of 200 m, possibly up to 320 m, from construction sites. We attribute the observed subsidence to load-induced, prolonged creep deformation of the sandy layers within the limestone, which is accelerated, if not instigated, by construction activities. Distant subsidence from a construction site could indicate extended sandy deposits. Anthropogenic and natural groundwater movements could also be driving the creep deformation. This study demonstrates that high-rise construction on karstic barrier islands can induce creep deformation in sandy layer within the limestone succession persisting for a decade or longer. It showcases the potential of InSAR technology for monitoring both building settlement and structural stability.

Key Points:

- We identify a widespread subsidence of up to 8 cm in the vertical direction over the 2016–2023 period in Sunny Isles and Surfside based on Sentinel-1 data
- There is a spatio-temporal correlation between new constructions in the area and subsidence signal
- The subsidence is likely due to prolonged creep deformation of sandy layers within the limestone, affected by construction activities

Supporting Information:

Supporting Information may be found in the online version of this article.

Correspondence to:

F. Aziz Zanjani,
fzanjani@earth.miami.edu

Citation:

Aziz Zanjani, F., Amelung, F., Piter, A., Sobhan, K., Tavakkoliestahbanati, A., Eberli, G. P., et al. (2024). Insar observations of construction-induced coastal subsidence on Miami's barrier islands, Florida. *Earth and Space Science*, *11*, e2024EA003852. https://doi.org/10.1029/2024EA003852

Received 9 JUL 2024
Accepted 23 NOV 2024
Corrected 6 JAN 2025

This article was corrected on 6 JAN 2025. See the end of the full text for details.

Author Contributions:

Conceptualization: Farzaneh Aziz Zanjani, Falk Amelung, Khaled Sobhan, Gregor P. Eberli

1. Introduction

The devastating collapse of the Champlain South Condominium Tower in Surfside, Florida, on 24 June 2021, claiming the lives of 98 individuals, has highlighted the need for monitoring of building stability, especially in coastal areas with corrosive environmental conditions. While the collapse was primarily attributed to the deterioration of reinforced concrete because of poor maintenance and design flaws (Logan & Singh, 2023), ongoing concerns persist regarding the potential impact of South Florida's coastal Karst environment on the structural integrity of buildings. South Florida's geology is generally characterized by young, highly porous limestone containing dissolution features like vugs, cavities, and sinkholes (Cunningham, 2004). But the geological situation of the barrier islands is complex because the limestone may contain interbedded sand layers. Interferometric Synthetic Aperture Radar (InSAR) data from the mid-1990s disclosed a land subsidence rate of −1.9 mm per year in the vicinity of the collapse site (Fiaschi & Wdowinski, 2020), raising the possibility of local geologic anomalies. To improve our understanding of coastal subsidence on South Florida's barrier islands and the impacts on building stability, we use InSAR data from modern, frequently revisiting satellite sensors which have been available since 2016. This paper is organized as follows. After providing the geological background (Section 2) and discussing the InSAR data processing approaches (Section 3) we present the InSAR results (Section 4), discuss the relationships between subsidence and new construction (Section 5) followed by a hypothesis about the subsidence mechanism (Section 6). The conclusions of this study are derived from data for individual buildings, which for the benefits of the residents are reported in considerable detail. Readers not interested in individual structures may skip several sections containing detailed data descriptions (Sections 4.3, 5 and 6.2).

Data curation: Farzaneh Aziz Zanjani, Falk Amelung, Andreas Piter, Amin Tavakkoliestahbanati
Formal analysis: Farzaneh Aziz Zanjani, Falk Amelung, Andreas Piter, Amin Tavakkoliestahbanati
Funding acquisition: Falk Amelung
Investigation: Farzaneh Aziz Zanjani, Falk Amelung
Methodology: Farzaneh Aziz Zanjani, Falk Amelung, Andreas Piter, Amin Tavakkoliestahbanati, Mahmud Haghshenas Haghighi, Mahdi Motagh, Pietro Milillo
Project administration: Falk Amelung
Resources: Farzaneh Aziz Zanjani, Falk Amelung
Software: Andreas Piter, Amin Tavakkoliestahbanati, Mahmud Haghshenas Haghighi, Mahdi Motagh, Pietro Milillo, Sara Mirzaee
Supervision: Falk Amelung
Validation: Farzaneh Aziz Zanjani, Falk Amelung
Visualization: Farzaneh Aziz Zanjani
Writing – original draft: Farzaneh Aziz Zanjani
Writing – review & editing: Farzaneh Aziz Zanjani, Falk Amelung, Andreas Piter, Khaled Sobhan, Amin Tavakkoliestahbanati, Gregor P. Eberli, Mahmud Haghshenas Haghighi, Mahdi Motagh, Pietro Milillo, Antonio Nanni, Esber Andiroglu

2. Geologic Background

The study area is situated on a barrier islands that are anchored on the northern end of the Pleistocene Florida reef tract (Banks et al., 2007). Although the main subsurface lithology of the barrier islands are stacked coralline limestone successions, variable amounts of molluscan grainstone and quartz sandstone interfinger with the reefal facies. These facies are heralding the barrier-beach and lagoonal facies that were the dominant lithologies further north (Enos & Perkins, 1977). On the shelf and west of the coral reef trend the Pleistocene Miami Oolite was deposited (Figure 1). The Miami oolite interfaces with the coquina of the Anastasia Formation to the north and the coralline Key Largo Limestone to the south. The Anastasia Formation comprises porous to very porous, sandy, shelly limestone, as well as nodular and shelly sandstone interbedded with sand (Fish & Stewart, 1991). In South Florida, the surface layer contains 30−40% quartz sands transported by longshore currents along the eastern coast of North America. Longshore transport and eolian transport produced the sandy layers within the limestone and the mixed carbonate and quartz sands in the subsurfacee Pleistocene successions.

Scott (2001) included the barrier island strata consisting of the coralline limestone and the intercalated molluscan and coral bearing carbonate sand and quartz sandstone layers into the Miami Limestone Formation (Figure 1). While Hoffmeister et al. (1967) included only two facies within the Miami Limestone: the bryozoan facies and the oolitic facies. The Miami Limestone exhibits a wedge-shaped structure with a maximum thickness of 13 m at its seaward edge (Evans, 1983). This limestone may contain alternating layers of harder and softer compositions and can feature a layer of remarkably dense and hard, light gray, freshwater limestone (Kaderabek & Reynolds, 1981). The highly porous, young limestone is characterized by dissolution features such as vugs, cavities, and sinkholes (Cunningham, 2004).

3. Data and Methods

Our data sources are 223 SAR images acquired by the European Sentinel-1 sensors between April 2016 and October 2023 (ascending track 48, spatial resolution 5 m in range and 20 m in azimuth directions), and 102 images of the German TerraSAR-X sensor between September 2017 and June 2021 (descending track 36, stripmap, spatial resolution 3 m in range and azimuth). We use the open-source ISCE2 stack processor for coregistering the SLCs using the orbit information. We then use persistent scatterer (PS) and distributed scatterer (DS) techniques to obtain time series of displacement. PS are point scatterers that are less affected by temporal and baseline decorrelation, resulting in high coherence throughout most of the study period. In a built environment examples for PS include balconies, air conditioning on rooftops and boardwalks along roads, all acting as corner reflectors. DS pixels contain the signal of multiple radar scatterers and show some temporal decorrelation. We employ both PS processing and a DS processing approach.

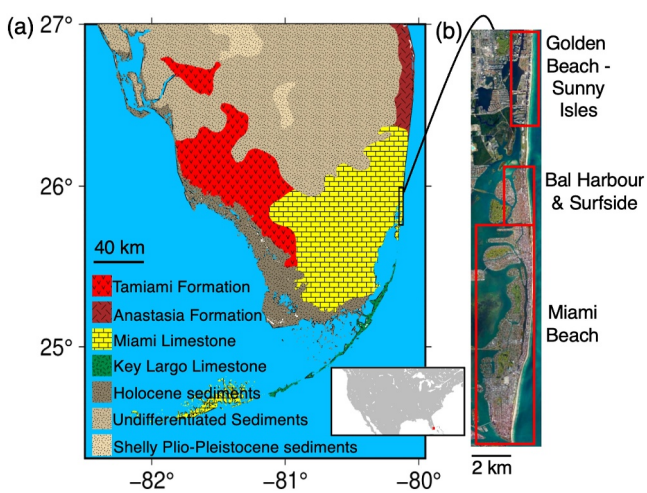

Figure 1. (a) Geologic map of Florida indicating formation boundaries following Scott (2001). Inset map shows the study area's location with red color. (b) The study area, outlined by the black rectangle in (a), is situated over the Miami Limestone.

For both PS and DS analysis, we first utilize the SARvey software, an open-source InSAR package for local-scale displacements detection (Piter et al., 2024a, 2024b). The PS analysis starts from a stack of co-registered, single-look complex images, prepared using the Miami Phase Linking software in Python (MiaplPy, Mirzaee et al., 2023). We compute interferograms based on a Delaunay network. In contrast to single-reference networks, we exploit the redundancy in the network and retrieve non-linear displacement signals without restriction to a temporal displacement model for unwrapping (Devanthéry et al., 2014). Unwrapping of the PS pixels is performed in a two-step approach. The PS pixels are selected with the Temporal Phase Coherence (TPC) approach (Zhao & Mallorqui, 2019). In the first step, we estimate the atmospheric phase screen (APS) from a small set of first-order points that exhibit exceptionally high temporal coherence. After removing potential outliers from the spatial network of first-order points, we unwrap their phases in time and space (Bioucas-Dias & Valadão, 2007; Boykov & Kolmogorov, 2004). The displacement time series is retrieved by inverting the interferogram network. In the second step, we select the final dense set of pixels for which the temporal coherence is higher than 0.8. We remove the APS from the points, unwrap their phase in time and space by connecting the second-order points with the first-order points and invert the network of

interferograms to retrieve the final phase time series. The overall processing chain for DS analysis in SARvey is similar to the PS analysis. The main differences are that we additionally filter the SLC based on self-similar pixels in the Miaplpy software and select DS pixels with phase linking coherence above 0.8.

The second PS approach evaluated in this study uses the SARPROZ software (Perissin et al., 2011). We conducted small area processing without APS filtering. We also use TerraSAR-X data to confirm the Sentinel-1 observations.

InSAR provides reliable data only for buildings that remain unchanged during the study period. However, along the Miami coastal strip, aging condominiums are constantly being replaced by modern ones resulting in the fading away of existing, and the appearance of new temporary persistent scatterers (Dörr et al., 2022). In order to obtain data for buildings that were completed prior to 2019, we therefore also consider a January 2019 to October 2023 period.

Throughout this paper we assume that all displacements are vertical and that 1 cm of LOS displacement corresponds to 1.36 cm vertical displacement (the radar incidence angle varies between 42.7 and 43). As the displacement histories are non-linear, we use averaged velocities, estimated by dividing the total displacements by the time period.

The location of a persistent scatterer on the ground depends on the range and azimuth coordinates and its height which is estimated from the InSAR data. The latter has uncertainties because of the narrow orbital tube of Sentinel-1 and because of phase-unwrap errors. Throughout most of this paper we therefore consider pixel locations assuming near-zero meters elevation (North American Vertical Datum of 1988), that is, 26 m below the WGS84 ellipsoid. The geolocation errors caused by this assumption are given in east and north directions by $x = H \cdot \cot\theta \cdot \cos\phi$, and $y = -H \cdot \cot\theta \cdot \sin\phi$, respectively, where H is the height of the persistent scatterer, θ the radar incidence angle, and ϕ the heading angle of the satellite (approximately 350°). For ascending data, a scatterer on a ∼100 m high rooftop therefore locates ∼110 m west and ∼20 m south of the structure. We used the SRTM DEM which in most parts of the study area has 5–10 m elevation. At a few locations where SRTM has 40–50 m elevation the above considerations do not apply, but these are not the subsiding buildings. With SARPROZ we processed the data twice, with and without DEM. In the DEM-assisted processing we have used a Lidar DEM. In the no-DEM processing we infer the height of the measured PS. These processing tests have been conducted to independently confirm the heights of our measurement points and to make sure we can distinguish whether a point is located on the roof or at the base of a building.

4. Detected Subsidence

4.1. Affected Structures

Figures 2–6 illustrate the LOS velocities from Golden Beach to Miami Beach and the displacement patterns for coastal structures undergoing subsidence using Sentinel-1 sensors and SARvey package. In addition to 2016–2023 periods, we consider the 2019–2023 period to include structures that were completed between 2016 and early 2019 because scatterers become persistent only after a structure is completed. Over the shorter period there are significantly more persistent scatterers than for the longer period. For this report, only the coastal strip has been carefully analyzed. There might be additional subsiding structures west of the coastal road which are not reported. Detailed information on the subsiding structures is summarized in Table S1.1, Section 1 of Supporting Information S1.

4.1.1. Sunny Isles Beach

In Golden Beach no subsidence is detected (Figure 2a). Figures 2b and 2c show the averaged velocities of scatterers for the Sunny Isles Beach North over the 2016–2023 and 2019–2023 period. The scatterers are located west of the structures because of the zero elevation assumption. There are no scatterers east of the structures because of the radar shadow from the buildings. Figures 2d–2k shows the displacement time series and the corresponding buildings in the area. During the 2016–2023 period, Ocean III and Bentley Residence development site exhibit LOS displacements of 4 cm. The Regalia, Ocean II, Marenas Beach Resort register 2–2.5 cm of displacement. For the 2019–2023 time period, the Armani Casa, Millennium condominium, and Porsche Design Tower display 4, 3, and 2 cm of LOS displacement, respectively. Note that TerraSAR-X detects over 10 cm of subsidence between 2017 and 2021 for Porsche Design Tower (see Section 2 in Supporting Information S1).

10.1029/2024EA003852

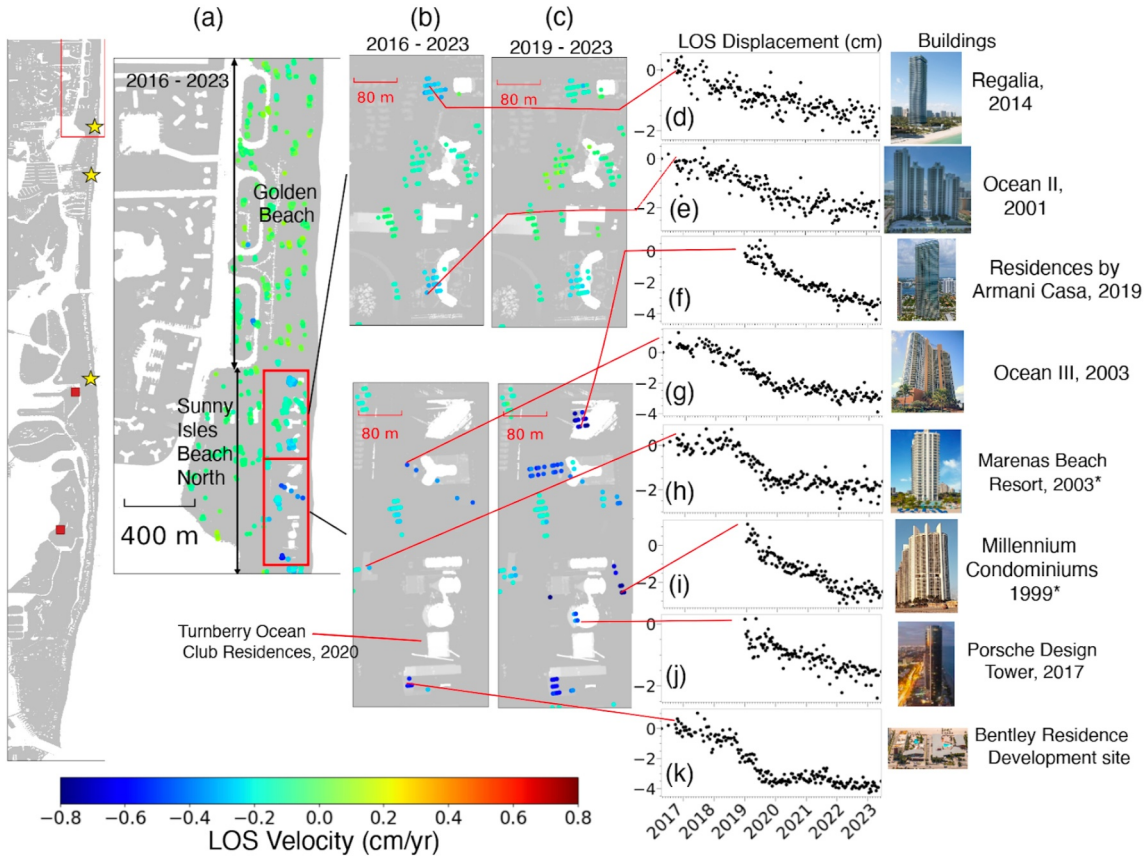

Figure 2. (a) Averaged 2016–Oct 2023 LOS velocity for Golden Beach and Sunny Isles Beach North, using Sentinel-1 sensors and SARvey package. Zoom-ins for (b) 2016–2023 and (c) 2019–2023, (d–k) LOS displacement time series for selected scatterers in these areas and the corresponding buildings. Years show the approximate completion date of the buildings. For each panel a local reference point is used. The pixels appear west of the structures because they are not geolocated using their estimated pixel heights. Vertical velocities can be obtained by multiplying with 1.36. (*): structures with uncertain pixels (see Table S1.1 in Supporting Information S1). Yellow stars and red squares show the location of boreholes in Figure 12.

Figure 3a shows the results for Sunny Isles Beach Central, with 3b and 3c comparing the scatterers for the two observation periods. Total of 13 structures exhibit subsidence in this area (Figures 3d–3p). Several properties, including the Mansions at Acqualina, Pinnacle, Chateau Beach Residences, Ocean Four Condominium, Jade Ocean Condos, show LOS displacements of 4–5 cm during 2016–2023 (Figures 3f, 3g, 3h, 3l, and 3n). During 2016 to 2023, Florida Ocean Club, Jade Beach Condos, and Jade Signature Condominium display approximately 3 cm of LOS displacement (Figures 3k, 3o, and 3p), while Double Tree Resort and Spa and Sole Miami, register 2.5 cm LOS displacements (Figures 3i and 3j). Over the 2019–2023 period, Acqualina Resort and Residences on the Beach, Trump International Beach Resort, and Muse exhibit 4, 3, and 2 cm of subsidence (Figures 3d, 3e, and 3m).

Similarly, Figure 4a displays the velocities for the Sunny Isles Beach South. Figures 4b and 4c show the results for both observation periods, and Figures 4d–4f exhibit the LOS displacements and the affected buildings. For this area, Trump Tower III suggests 4 cm of subsidence during 2016–2023. The Ritz Carlton Residences exhibits large subsidence of 5 cm during 2019–2023, while Kings Point Imperial Condo has less than 2 cm of LOS displacement.

4.1.2. Bal Harbor and Surfside

Figures 5a–5c represent LOS velocities for Bal Harbor and Surfside area. Figures 5d–5o illustrate the LOS displacement for the affected structures. Over the 2016–2023 period, the Surf Club Towers exhibit 3–4 cm of LOS displacement (Figures 5k–5m), the Oceana complex displays 4.5 cm (Figure 5d), the Marbella Condominium, Waverly, Carlisle on the Beach, Residence Inn, Luxury condo, and Fendi Chateau Residence show 1–1.5 cm of

10.1029/2024EA003852

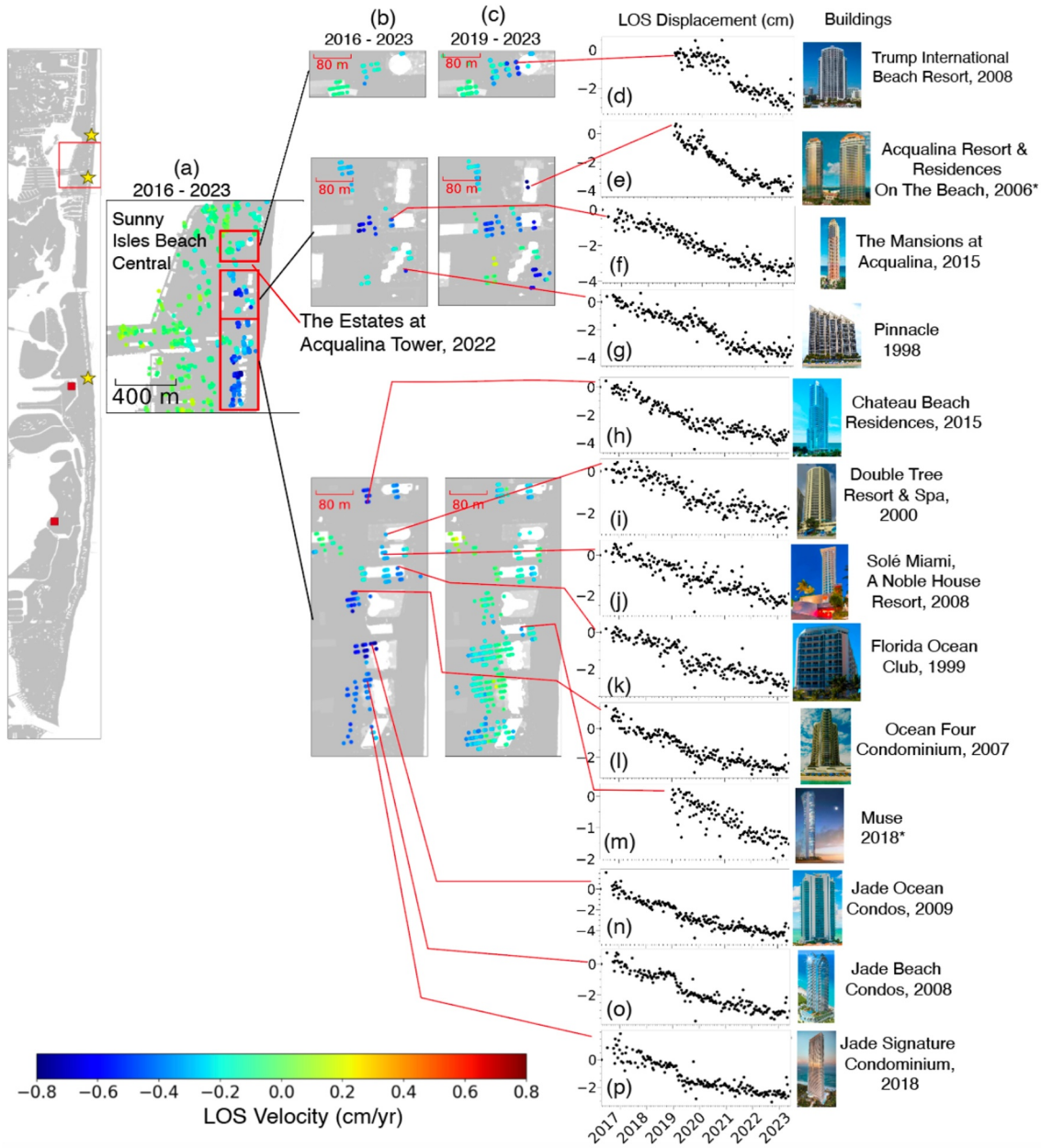

Figure 3. Same as Figure 2 but for zoom-ins in Sunny Isles Beach Central.

LOS displacement (Figures 5f–5j). Over the 2019–2023 period, the Arte condominium and the 87 Park Tower display ∼3 cm of LOS displacement (Figures 5n and 5o). The latter is situated south of the collapsed building in Miami Beach, but for simplicity we consider it to be part of Surfside.

For the Champlain Tower South we did not find any evidence for precursory displacements prior to the 2021 collapse but the results are inconclusive because the section of the structure where the collapse initiated can not be imaged from space (see Figure S1.1 in Supporting Information S1).

Note that the southern part of the Fendi Residence and the northern part of the Surf Club North Tower (Figure 5b) show slightly higher averaged velocities than the northern and southern parts of the respective structures (by 0.2–0.3 cm/yr), which is discussed in Section 6.4.

10.1029/2024EA003852

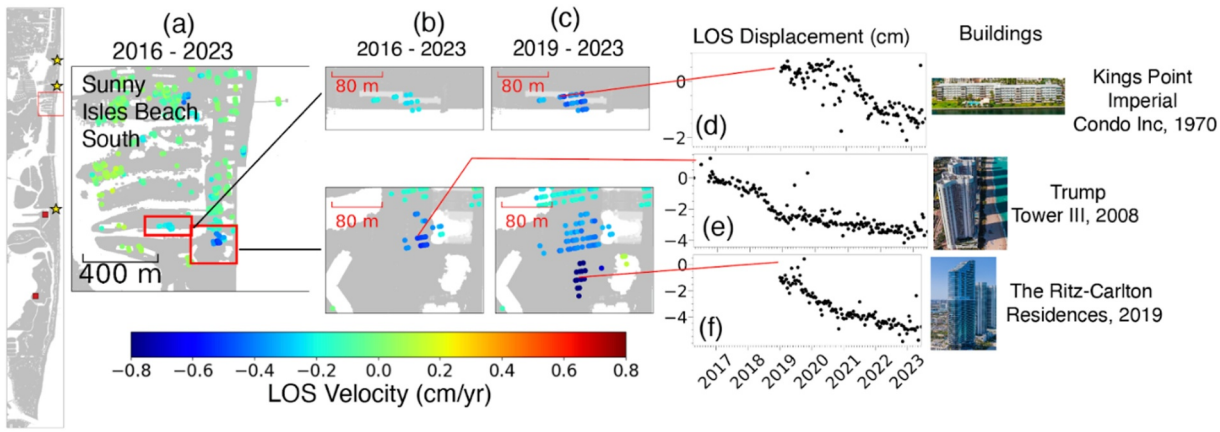

Figure 4. Same as Figure 2 but for zoom-ins in Sunny Isles Beach South.

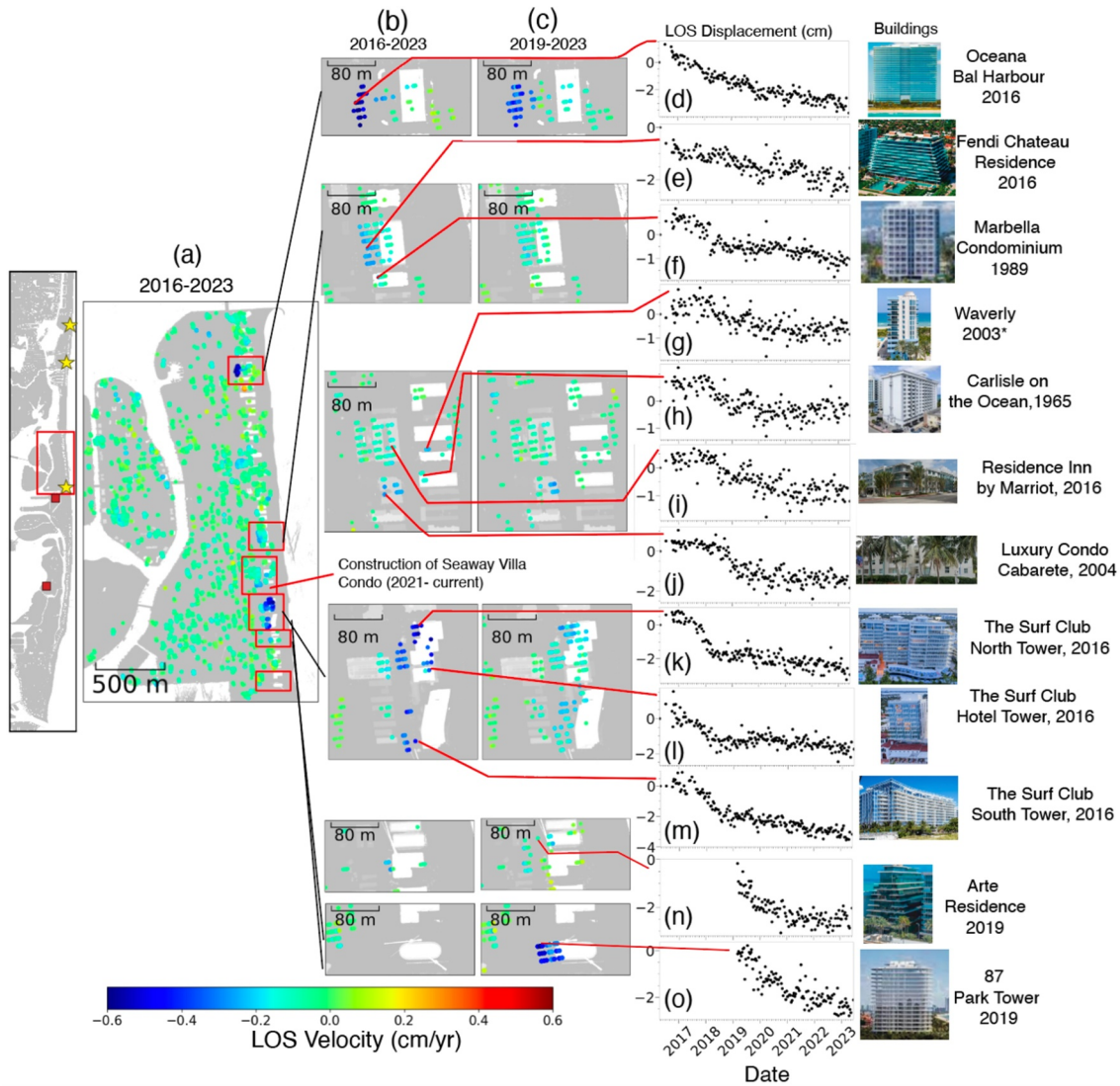

Figure 5. Same as Figure 2 but for Bal Harbor and Surfside.

10.1029/2024EA003852

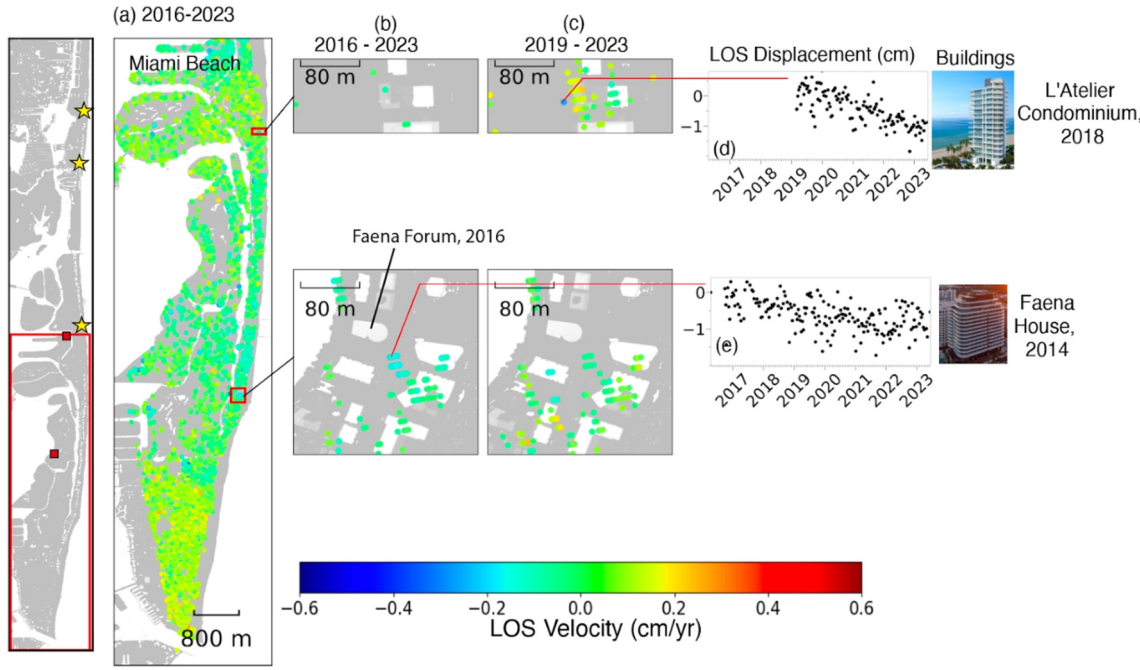

Figure 6. Same as Figure 2 but for Miami Beach.

4.1.3. Miami Beach

In Miami Beach we do not observe much subsidence. The exceptions are the L'Atelier Condominium which shows 1–1.5 cm of displacement during the 2019–2023 timeframe and the Faena House which displays 1 cm of displacement during 2016–2023 (Figure 6). The Faena Forum constructed in 2016 has no scatterers due to the shape of the building.

4.2. Temporal Subsidence Patterns

The signals exhibit two distinct temporal patterns, though our classification is simplified for clarity. The first pattern shows an exponential decline in subsidence over the entire observation period. This decline may occur rapidly, with 2–4 cm of subsidence within the first 1–2 years, or it may occur more gradually including subsidence at a near-constant rate. The second pattern entails a sudden onset or acceleration and subsequent decline of subsidence. It is important to note that while this classification captures the general behavior of the time series, there are cases where the observed subsidence may include inflection points that complicate the categorization.

Examples for the first pattern include Armani Casa, Ritz-Carlton in Sunny Isles Beach (Figures 2f and 4f); the Surf Club Towers, Arte and 87 Park in Surfside (Figures 5k–5o) and with more gentle decay Chateau Beach in Sunny Isles Beach (Figure 3h), Oceana and Fendi in Bal Harbor (Figures 4d and 4e).

Examples for subsidence at near constant rate include Regalia, Sole Mio and Muse in Sunny Isles Beach, Fendi in Bal Harbor, and L'Atelier and Faena House in Miami Beach (Figures 2d, 3j, 3m, 5e, 6d, and 6e).

Examples for the second pattern include Ocean III, Marenas, and Trump International in Sunny Isles Beach (Figures 2g, 2h, and 3d) and Marbella and Cabarete in Surfside (Figures 5f and 5j), and the Bentley site, all three Jade structures and Trump Tower III for acceleration of subsidence (Figures 2k, 3n, 3o, 3p, and 4e). The temporal patterns are summarized in Table S1.1 of Supporting Information S1.

However, we acknowledge that some cases within this first pattern, such as the time series of Figures 5k–5m, display a more complex, punctuated history, with sharp breaks or inflection points (e.g., around 2018). These features may suggest a transition between rapid and slow phases, which aligns more closely with the second pattern —a sudden onset or acceleration followed by a subsequent decline of subsidence—with the onset potentially occurring before the recorded time series.

Note that the second pattern also has exponential characteristics and that it can be described as the superposition of two exponentially decaying signals with different decay constants, amplitudes and phases.

4.3. Distributed Scatterers

Figures 7 and 8 contrast the averaged velocities obtained from the DS with those from the PS for the 2016 to 2023 timeframe. The DS approach provides data for much more pixels albeit with higher uncertainty, which allows us to better assess the spatial extent of the subsidence. The PS approach provides data only for highly coherent point scatterers. In the remainder of this paper we refer to the structures using abbreviated names.

In Sunny Isles Beach, the DS data identify four notable subsidence areas, which we name according to structures built during our study period (Figure 7): The Armani-Porsche-Turnberry hotspot which refers to a collective grouping of three distinct structures (hotspot A), the Estates-at-Acqualina-South Chateau- Mansions (hotspot B), Muse-Jade-Signature (hotspot C), and Ritz Carlton (hotspot D).

In Surfside and Bal Harbor (Figure 8), the DS data identify a subsidence hotspot with 325 m in along-shore length and 200 m width in the Surf Club area (hotspot E). On the other hand, subsidence of the Oceana, Arte and the 87 Park Tower is restricted to the buildings themselves.

The collective findings from both DS and PS analyses is that for most sites subsidence extends into the surroundings of a high-rise, while for some sites subsidence is confined to the built structure.

4.4. Location Uncertainties

Figure 9 shows for the subsiding structures in Bal Harbor and Surfside the LOS velocities at locations calculated assuming near-zero meters scatterer elevation, at locations calculated using the estimated scatterer elevations, the estimated scatterer elevations themselfs, and the actual elevation of the structures given by a lidar-derived digital surface model (DSM). The DSM model was acquired between May and November 2018 when 87 Park Tower and Arte were under construction as indicated by the presence of construction cranes (Figures 9e5 and 9f5).

For Oceana (height ∼90 m) the subsiding scatterers are located ∼80 m west of the structure (Figure 9a1) as expected for scatterers on or near the rooftop. The estimated elevations of ∼80 m (Figure 9a3) of these pixels match the DSM (Figures 9a4, and 9a5). The same applies for the Fendi, for the Surf Club North and South structures and Arte with estimated elevations of ∼45 m (Figures 9b4, 9d4, 9e4, 9b5, 9d5, and 9e5). For 87 Park Tower the estimated elevations of ∼60 m are consistent with an 18-story structure (Figure 9f4). The DSM has lower elevations (Figure 9f5) but this is because the DSM was acquired before the structure was completed. For the Carlisle the estimated elevation of ∼35 m agrees with the building height, as does the estimated elevations for the Residence Inn and Cabarete (4 and 3 stories high, estimated elevations of ∼15 m). For Marbella, the estimated elevation of ∼30 m approaches the building height. For these 10 structures the scatterers are clearly located on the rooftops. However, for the Waverly and the Surf Club Hotel, the estimated elevation of the subsiding scatterer of ∼0 m (Figures 9c4, 9d4, 9c5, and 9d5) puts in question whether the scatterers are located on the rooftop.

Some of the structures have pixels that appear within their footprints, but the estimated elevations are less than the building height (Oceana, Fendi, Surf Club North, 87 Park). The scatterers may be situated at lower levels on the building facades, but it is also possible that these pixels contain signals from two scatterers located at different elevations, multipath reflections or a combination of these effects. Layover effects complicate urban InSAR studies (Ma et al., 2021; Yang et al., 2019). Alternatively, the estimated elevations could be incorrect because of phase unwrapping errors.

For Oceana the pixels with ∼0 m elevation (green-yellow colors, Figure 9a3) could represent scatterers within the structure's opening in the lower 4 stories (Figure 9a4). For Fendi and 87 Park Tower, pixels with low elevations are situated in the western sections, suggesting that the scatterers are located at different levels along the facade.

In Sunny Isles Beach, the Ocean III, Millennium, Trump International Beach, Bentley site, Pinnacle, Florida Ocean Club, and Kings Point have pixels that agree in elevation with the height of the buildings (see Section 1 in Supporting Information S1). We can be certain that these scatterers are located on the rooftop. These structures are of elevation up to 110 m (Table S1.1 in Supporting Information S1). For most structures with height up to 200 m, the persistent scatterers are located 20–50 m west of the structure, that is, the scatterers are located on the west facades and not on the rooftops. Structures of this height are more difficult to study. For Miami Beach, both the

10.1029/2024EA003852

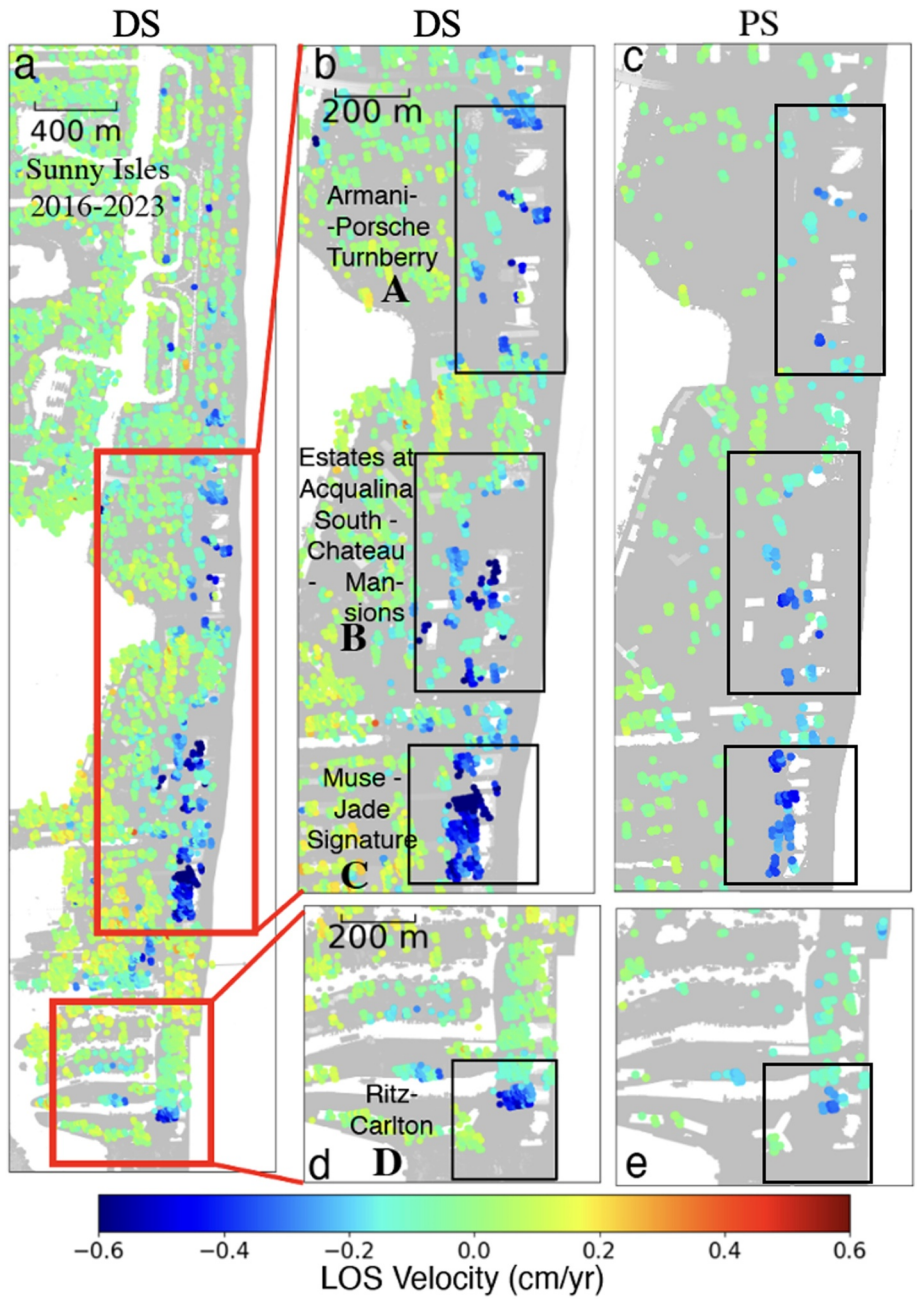

Figure 7. Combined PS and DS for Sunny Isles for 2016–2023 timeframe. Zoom in plots show the comparison of DS and PS results. DS results show more scatterers with subsidence pattern and contains PS scatterers as well.

L'Atelier Condominium and Faena House show scatterers on the rooftop (see Section 1 in Supporting Information S1).

4.5. Validation Using TerraSAR-X and the SARPROZ Software

The most challenging aspect of InSAR processing is phase-unwrapping, in particular in urban environments with significant layover effects. To ensure that our results are not dominated by phase unwrapping errors, we validate the outcomes obtained using SARvey for selected structures with the well-established SARPROZ software, which employs a different processing strategy. For this validation, we use both Sentinel-1 and TerraSAR-X data, noting that TerraSAR-X data is available for a shorter time period (Figure 10).

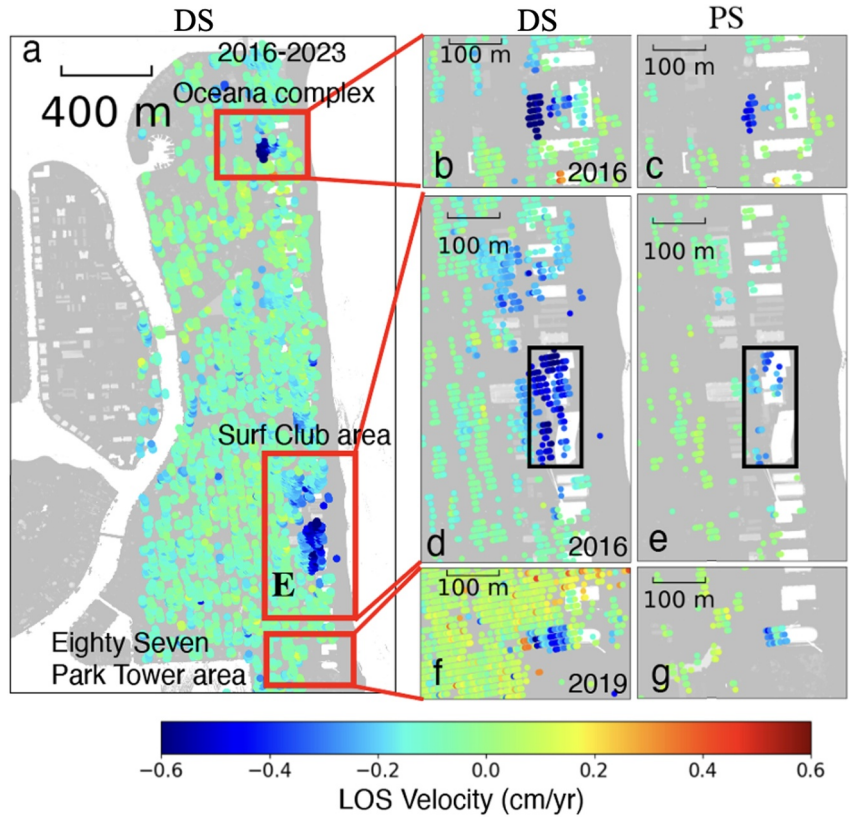

Figure 8. Same as Figure 7 but for the Surfside and Bal Harbor area with zoom-ins on the Oceana Residence, Surf Club Hotel areas, and 87 Park Tower. All data are for the 2016–2023 timeframe except for 87 Park Tower area. The black box is for visualization of the spatial extent of the signal around Surf Club Towers.

For the Oceana building in Bal Harbor and Surf Club North Tower (Figures 10a and 10b), both Sentinel-1 and TerraSAR-X satellites exhibit congruent findings. Similar pixels on the rooftops are identified from SARPROZ and SARvey results, facilitating a comparison of their respective time-series data. There is a good agreement in LOS displacement for the period where the results overlap (September 2017 to mid-2021). Additional time-series of TerraSAR-X data for Sunny Isles Beach are shown in the Section 2 of Supporting Information S1, noting that we could not identify same scatterers with similar locations. The TerraSAR-X indicates 10–12 cm of LOS displacement for Porsche Design tower. When comparing TerraSAR-X and Sentinel-1 for this building, it appears that a portion of the LOS displacement might be attributed to horizontal movement which requires detailed investigation.

We note that a contractor report by the National Institute of Standards and Technology confirms subsidence in the Muse-Jade Signature subsiding area (area C in Figure 7, Saidi et al. (2024)).

5. Relationships Between Age, Height of Structures and Subsidence Signal

5.1. Age of Impacted Structures

We have determined the completion years of all structures using Google Earth imagery (see Section 3 in Supporting Information S1). From the 35 subsiding structures, 7 were constructed in the previous century (Millennium and Bentley site in Figure 2; Pinnacle and Florida Ocean in Figure 3; Kings Point in Figure 4; Marbella and Carlisle in Figure 5), 13 between 2000 and 2014 (Ocean II, Ocean III, and Marenas in Figure 2; Trump International, Acqualina Resort, Double Tree, Sole Miami, Ocean Four, Jade Ocean, and Jade Beach in Figure 3; Trump Tower III in Figure 4; Waverly and Cabarete in Figure 5), 12 just before or during the early years of our data (after 2014, Regalia, and Porsche Design in Figure 2; Mansions at Acqualina, Chateau Beach Residences, Muse, and Jade Signature in Figure 3; Oceana, Fendi, Residence Inn, Surf Club in Figure 5, L'Atelier and Faena

10.1029/2024EA003852

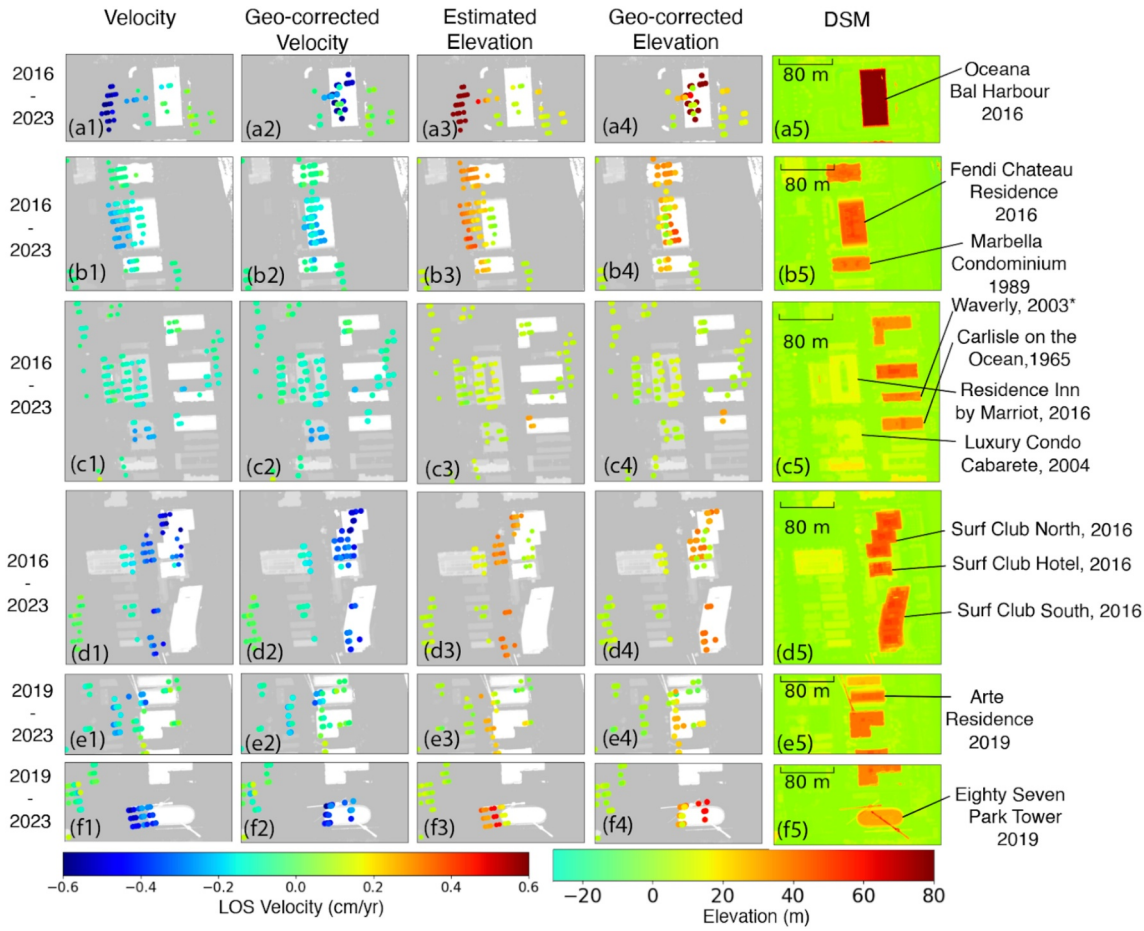

Figure 9. Velocity, geo-corrected velocity, estimated elevation based on DEM error, geo-corrected estimated elevation, DSM for the Surfside and Bal Harbor. First column is the time-period of observation for each box.

House in Figure 6); and 3 during the periods covered by our data (Armani Casa in Figure 2; Ritz Carlton Residences in Figure 4; and the 87 Park Tower in Figure 5).

5.2. Structures Completed During Observation Periods

The Jade Signature was completed in 2018 and the Armani Casa, Ritz Carlton and the 87 Park in 2019. We would not expect any data because no persistent scatterers were active during the entire 2016–2023 and 2019–2023 periods, respectively. There are two possible explanations for our observations in the respective timeframes. First, the absence of persistent scatterers at the beginning of the periods does not impact the amplitude dispersion enough to reject these pixels as persistent scatterers. Alternatively, the persistent scatterers can be situated on the facades of these buildings and became active before construction was completed. The noise at the beginning of the time series for these structures (Figures 2f, 3p, and 4f) suggest the former explanation.

The three structures that were completed since 2020, the Turnberry, the Estates at Acqualina South, and Marinas lack data due to the absence of persistent scatterers.

5.3. Structures Without Data

The Millennium and Acqualina Resort & Residences which were completed in 1999 and 2006, respectively, do not have data in the 2016–2023 timeframe. The reasons why there is no persistent scatterers active during the entire period is unknown. These structures do have data in the 2019–2023 timeframe.

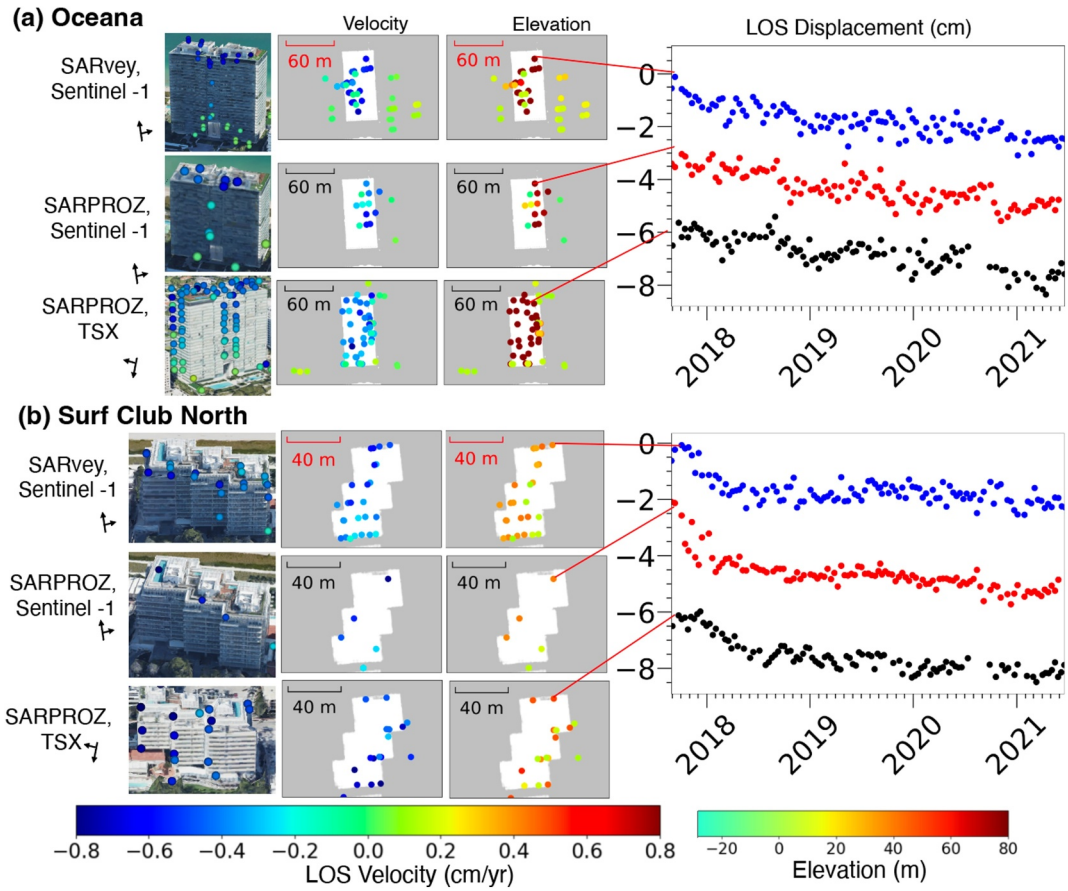

Figure 10. Comparison of SARvey Sentinel-1, SARPROZ Sentinel-1, and SARPROZ TerraSAR-X results for (a) Oceana, (b) Surf Club North.

5.4. Structures Completed Since 2014 Without Subsidence

The Grand Beach Hotel in Surfside is a structure that was completed in 2016 but does not show subsidence (Section 1 in Supporting Information S1).

5.5. Height of Impacted Structures

In Sunny Isles Beach, most of the brand-new subsiding structures (since 2014) have an elevation of 150–200 m, the early 21st century (2000–2014) subsiding structures of 100–150 m while most of the older ones (~pre-2000) are of lower elevation. In Bal Harbor the Oceana has an elevation of 100 m while in Surfside where the maximum condo height is 12 stories, the typical elevation is 50 m. The condo elevations are summarized in Table S1.1 of Supporting Information S1. While higher structures generally exhibit more subsidence there are many buildings not fitting this trend (Figure 11). Most notably, four low-rises with elevation less than 20 m (Bentley development site, Kings Points, Residence Inn and Carbarete) experience ~2–3 cm subsidence.

6. Discussion

We have observed subsidence at 33 out of the 87 coastal structures in Sunny Isles Beach, Bal Harbor and Surfside (Table 1) ranging from 1.5 to 6 cm in the LOS direction, equivalent to 2–8 cm vertically (See Table S1.1 in Supporting Information S1). Care has to be taken when comparing total subsidence between buildings because of varying time spans. We also identified one building in Sunny Isles South and two in Surfside that show subsidence but are not directly located at the coast. As Table 1 shows, subsidence is particularly widespread in Northern and Central Sunny Isles Beach where 67% of the existing structures are subsiding. In Surfside, 9 out of 27 coastal buildings show subsidence. In Sunny Isles South and Bal Harbor, only 2 out of 13 and 1 out of 18 structures are

10.1029/2024EA003852

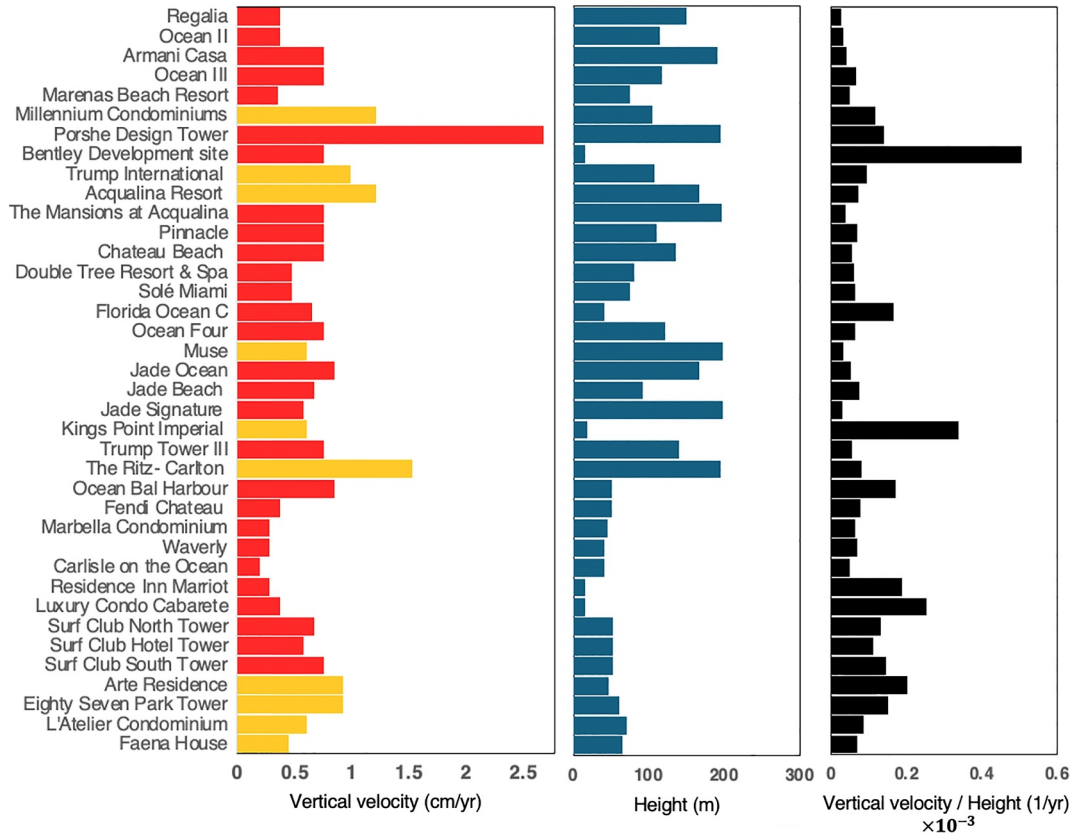

Figure 11. Summary of subsidence observations and comparison of rate of subsidence for each building with the height. Red and orange colors show subsidence for 2016–2023, and 2019–2023, respectively. For Porsche Design tower, we used the rate from TerraSAR-X, which covers 2016–2021 time period (Section 2 in Supporting Information S1).

subsiding, respectively. Further south in Miami Beach there are ~110 coastal structures, but only 2 show a very subtle, localized subsidence signal (0.5 and 1.5 cm LOS displacements over the 6.5-years period).

Given that groundwater pumping is absent in the study area, a common factor often attributed to urban land subsidence (Amelung et al., 1999; Chaussard et al., 2021), and that limestone does not undergo long-term settlement— a phenomenon typically associated with fine-grained soils related to fluid expulsion— what could be the underlying cause for the observed subsidence? We now explore the temporal patterns of the observed

Table 1
Total Numbers of Coastal Structures Derived From Google Earth Imagery and Numbers of Subsiding Structures in Different Sections of the Northern Miami Barrier Island

	# Of coastal structures			# Of structures showing subsidence		
Location	Total	Completed since 2014	Completed since 2020	Total	Completed before 2014	Approx. Average height of new buildings [m]
Sunny Isles (North)	12	4	1	8	5	185
Sunny Isles (Central)	19	5	1	13	9	186
Sunny Isles (South)	13	1	0	2	1	195
Bal Harbor	16	1	–	1	1	100
Surfside	27	8	1	9	3	50
Total	**87**	**19**	**3**	**33**	**16**	–

Note. For the counts only first-row ocean front properties are considered (the Residence Inn in Surfside and Kings in Sunny Isles South has been excluded).

subsidence, proximate construction activities and geological characteristics to elucidate the underlying causes of the observed subsidence.

6.1. Spatio-Temporal Relationship of Subsidence With New Construction

The buildings experiencing exponential decay to constant rate subsidence were constructed right before or at the start of the observation periods. We now show that there is also a spatial-temporal correlation between subsidence and construction timelines: the sudden onset of subsidence occurs at times of nearby construction, in particular for the older structures.

Examples of sudden onset of subsidence coinciding with nearby construction are observed in Sunny Isles in early 2018 at the Marenas and the Bentley site (Figures 2h and 2k) when the Turnberry Ocean Club was constructed at 40–60 m distance (see Table S1.1 in Supporting Information S1); in mid-2017 at the Ocean III (Figure 2g) when the Armani Casa was being constructed (distance ~50 m); in late 2019 at the Pinnacle (Figure 3g) when the Estates at Acqualina was constructed ~300 m to the north; in 2021 at Trump International (Figure 3d) when the Estates at Acqualina was still under construction (distance ~70 m); in early 2019 at all three Jade structures (Figures 3n, 3o, and 3p) when both Muse and Jade Signature were under construction in the area (at distances between 20 and 200 m); in early 2019 at Trump Tower III (Figure 4e) when Ritz-Carlton was under construction (distance <40 m); and in early 2021 at Kings Point (Figure 4d) when La Marinas and Marina Del Sol were under construction in the vicinity. Examples in Surfside are observed in 2018 at the Carlisle and Residence Inn and Cabarete (Figures 5h, 5i, and 5j) while Arte Residences ~400 m to the south was built. We reiterate that we report temporal correlations only which may or may not indicate a causal relationship.

Some of these structures were already undergoing gradual subsidence when subsidence accelerated, such as Bentley site (Figure 2k), the Pinnacle, Florida Ocean, Ocean Four, and all three Jade structures (Figures 3g, and 3k–3p), and Trump Tower III (Figure 4e). Nearby construction prior to the study period near the Pinnacle includes the Mansions at Acqualina and Chateau Beach Residences that were built in 2011–2015 and 2013–2015, respectively (distances of 45 and 80 m), and near the Jade structures, the Chateau Beach Residences (distance 300–500 m). An older building showing subsidence during the entire period is the Millennium (Figure 2i) with the Porsche Design Tower constructed in its vicinity during 2011–2017.

Major new construction not only affects nearby structures but also the entire surrounding area, which exhibits signs of subsidence. The five subsidence areas (labeled A, B, C, D, and E in Figures 7 and 8) are named after structures with construction timelines consistent with the observed subsidence. This correlation further strengthens our conclusion that subsidence is related to construction activities. The observed spatio-temporal correlation suggests that construction activities can impact existing structures within a distance of 200–300 m. For example, structures around Muse and Jade Signature showing subsidence are within 200 m. Chateau with slow exponential decay is 320 m away from Muse. Pinnacle is 250 away from The Estates at Acqualina. In addition, the along-shore extent of area A is about ~650, with major constructions such as Porsche and Turnberry at its center. Distances from nearby construction sites relative to subsidence signals are also given in Table S1.1 of Supporting Information S1.

6.2. Correlation With Shallow Geologic Structure

Geotechnical reports summarizing subsurface exploration programs typically consisting of soil and rock sampling for laboratory testing provide information on the shallow geological structure. In the northern section of the study area at the Porsche Design Tower, a 50 m deep exploration drill hole reveals that the limestone base is topped with approximately 7 m of sand and includes four distinct sand layers of 2–5 m thick. Sandy layers constitute 50% of the stratigraphic sequence (Figure 12a). A drill hole at the Muse Residences located 1.5 km further south also identifies deeper sand layers, but they make up only about 20% of the strata beneath the top sand layer (Figure 12b). Further south in Surfside, a 35-m deep drill hole for the 87 Park Tower identifies only one 1.5 m thick sand layer below the shallow sand layer (Figure 12c), and the drillhole beneath the L'Atelier condominium in Miami Beach lacks any interbedded sand layers below the shallow sand layer (Figure 12d), but it reaches only to 25 m depth. For more comprehensive data derived from the geotechnical reports see Section 4 in Supporting Information S1. The reports also provide the N-values from the Standard Penetration Test (SPT) which provide estimates for the shear strength of the sandy layers and for the consistency of the limestone.

10.1029/2024EA003852

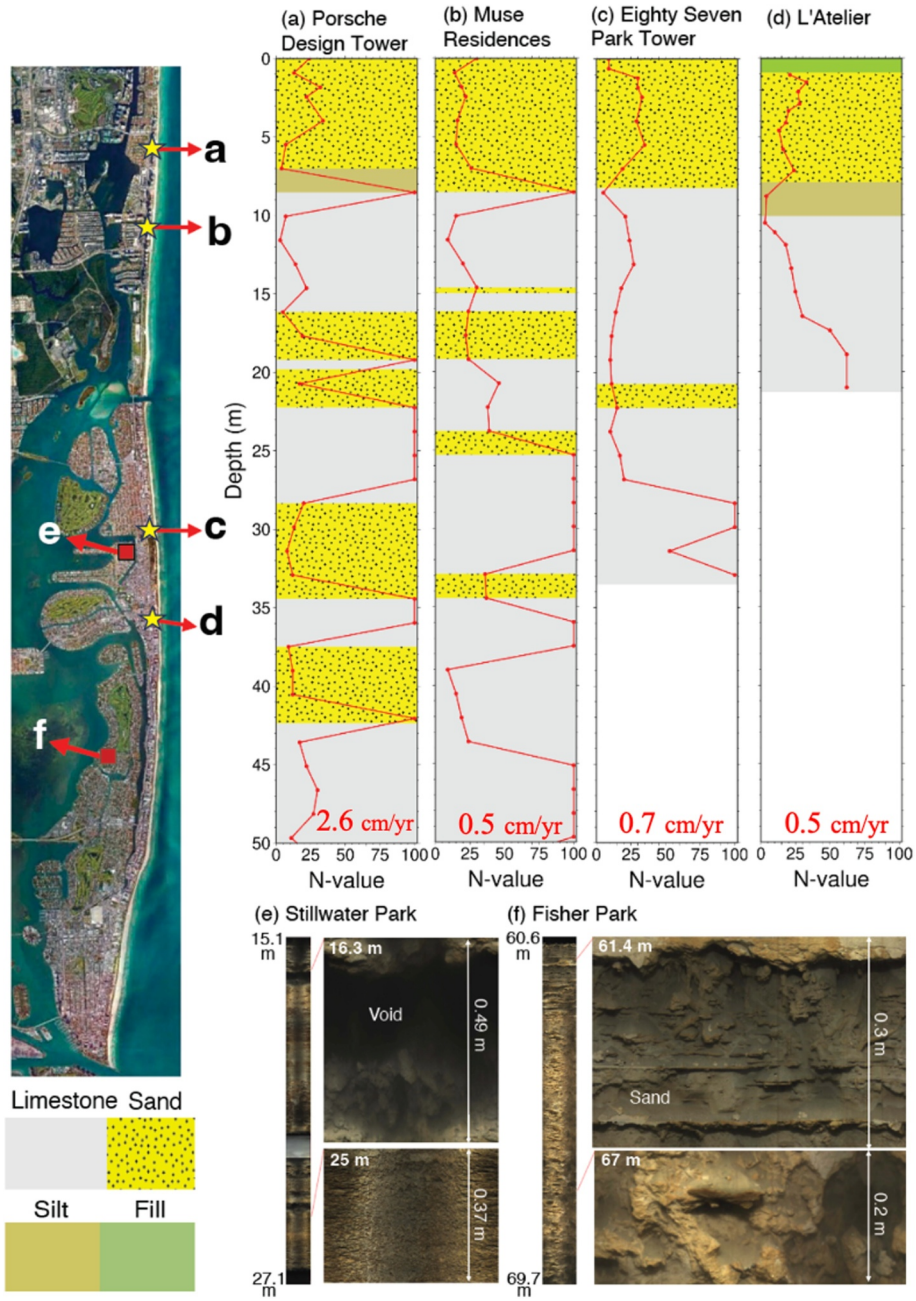

Figure 12. (a–d) Subsurface geology based on available geotechnical reports from public records of Surfside and Sunny Isles. N-value is the number of blows needed for penetration of a tube over a specific depth, indicating soil resistance. (e, f) Sections of boreholes from USGS logs in Miami Beach showing embedded sand at 63 m depth and a 0.3 m void at 14 m depth. The observed LOS displacements are over 10 cm during 2017–2021 for Porsche Design tower Tower (from TerraSAR-X, see Section 2 in Supporting Information S1), and 2, 3 and 2 cm during 2019–2023 for Muse, 87 Park and L'Atelier, respectively. Red numbers below each profile show the approximate LOS velocity in cm/yr.

The occurrence and magnitude of subsidence appears to strongly correlate with the presence of sandy layers in the underlying strata. Notably, the area surrounding the Porsche Design Tower where the underlying limestone contains about 50% sandy layers, exhibits significant subsidence (hotspot A on Figures 7, 8 cm vertical), while at the 87 Park Tower with less sandy layers, subsidence is less and confined to the structure itself (4 cm vertical). Further south under Miami Beach, no sand layers have been identified and the limestone is relatively hard as indicated by high SPT N-values (Figure 12d), consistent with the small and localized subsidence observed in this

area. The absence of sandy layers may also explain why two of the newly built structures (Grand Beach Hotel in Surfside and Faena House in Miami Beach, built since 2014) do not subside. Alternatively, construction practices that do not lead to subsidence may have been employed at these structures.

The surficial sandy layer has been accumulated during the formation of the barrier island and contains both carbonate and quartz sands. The sands interbedded in the limestone are quartz sands and likely transported to the area by longshore transport.

Optical images from two boreholes (USGS, 2000) provide visuals of the shallow geology and its variability under the barrier island. Stillwater Park shows a 0.5 m void at 16 m depth and solid limestone at 25 m depth (Figure 12e), while the Fisher Park drill hole provides examples for sandy layers at 61.4 and 67 m depth (Figure 12f). These images are evidence for the presence of sandy layers and voids in the hard limestone to depths larger than 60 m, which we interpret to be responsible for the observed subsidence.

6.3. Long-Term Creep Deformation of Interbedded Sand Layers

Our observations reveal subsidence persisting for over 8 years post-construction. However, in Miami's limestone we would expect instantaneous settlement during construction followed by a few months of post-construction settlement. This short-term settlement is caused by the crushing of voids due to the installation of deep foundations such as driving pile groups or installation of cast-in-situ drilled shafts and subsequent application of structural loads (McDowell & Khan, 2003).

A potential explanation for the observed long-term (multi-year) subsidence signal is creep deformation of the sand layers interbedded in the limestone. Here we discuss three mechanisms that could cause this deformation. Brittle or ductile creep within the rock matrix could be an alternative mechanism but we consider it unlikely because it is a slower process.

6.3.1. Construction Vibrations

Granular media, such as sand layers, are known to be highly sensitive to vibrations. In our study area, intense vibratory actions have been employed for the construction of at least two structures, the 87 Park Tower and the Porsche Design Tower. At the latter, a range of construction activities— including the demolition of old structures, extraction of existing piles, vibratory installation of interior and exterior sheet pile walls, installation of anchor sheet pile walls, and construction of auger cast piles for new foundations—began in 2013. The vibrations at these structures have been associated with dynamic settlement-induced structural damage in nearby structures, which has been subject to legal investigations (Logan & Singh, 2023; Sobhan & Reddy, 2015).

The mechanism for subsidence due to construction-induced vibrations is sketched in Figure 13. The grains within the interbedded sand layers reconfigure to a denser packing in response to the sustained structural load and the dynamic loads from the vibrations (Figures 13b, and 13c). The accommodation of the cyclic vibratory shear strain by matrix of sand particles leads to the closure of holes by particle rearrangements and volume reduction of the sand (Youd, 1977). This process is known as dynamic settlement leading to the subsidence that is observed and measured at the surface. It is aggravated by the presence of a sustained load. Once the construction vibrations have ceased, particle rearrangement may still continue under the sustained load due to a phenomenon known as creep (Figure 13d, e.g. Kuwano & Jardine, 2002; Lade, 1994; Lade & Liu, 1998; McDowell & Khan, 2003). Dynamic settlement and subsidence can be caused by relatively weak vibratory actions (K. Massarsch, 2000; K. R. Massarsch & Fellenius, 2014).

But why does settlement continue for years after vibrations have stopped? Research by Henann and Kamrin (2014) into the behavior of sand as a dense granular medium demonstrated that shear deformation within a specific area can lead to the fluidization of the entire medium, effectively eliminating the yield condition across the board. This fluidization allows for the slow creep deformation of areas that are otherwise considered to be in a static state when an external force is exerted on a probe. It suggests that vibrations from pile-driving similarly influence the behavior of sand layers interbedded within the limestone formations, and that fluidization is maintained to some degree once it has been initiated.

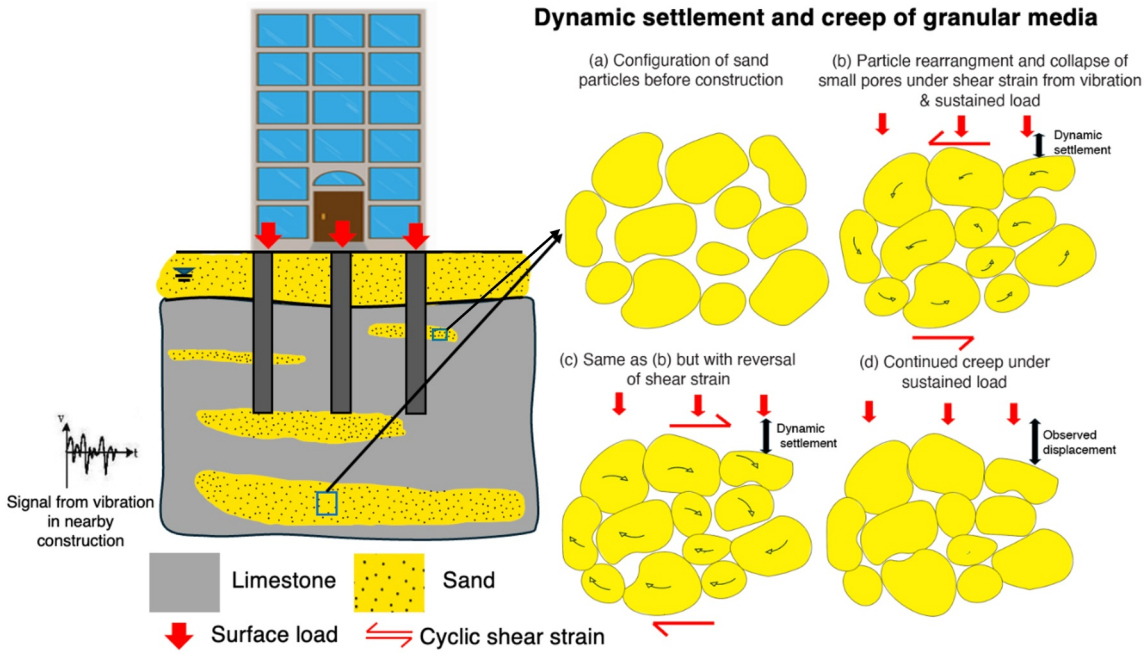

Figure 13. Schematic illustrating potential scenario to explain the observed subsidence pattern. (a) Sand particles prior to construction, (b, c) creep and dynamic settlement of sand layers within limestone under the load of the building & vibration. (d) Continued creep of sand layers under the load. The cyclic tidal flow could also lead to particle rearrangement.

6.3.2. Construction Pumping

Builders make efforts to limit construction vibrations, which are carefully monitored during construction, and, if the measured peak particle velocity (PPV) exceeds a threshold value, construction is halted to prevent damages to nearby structures. Another mechanism of how construction activities can cause subsidence is the drawdown of the water table for the construction of the foundation and underground garages. The movement of groundwater in response to the pumping can lead to particle rearrangement within the sandy layers and induce similar effects as vibrations.

6.3.3. Tidal Flow and Stormwater Injection

While construction activities are a plausible explanation for the observed subsidence with an exponential decay, the mechanism causing subsidence at constant rate is more puzzling. A possible explanation are tidal-driven groundwater movements which are also associated with cyclic strains similar to construction vibrations. The structural load of a new coastal high-rise may lead to channeling of the tidal flow, locally enhancing the tidal flow's ability to change the packing of the sand grains. Another possible explanation is the injection of stormwater into the subsurface, which is practiced at most high-rises for flood management. There are three ways how stormwater injection can lead to subsidence. First, the movement of groundwater in response to pressure increase can lead to grain rearrangements similar to tidal flow. Second, channeled groundwater flow could mobilize sandy grains and transport them elsewhere. Third and most importantly, the injection of freshwater can lead to the dissolution of the limestone. While the dissolution of solid limestone is slow, the dissolution of fine carbonate sands is a much faster process and can cause subsidence of 1 mm/yr or more. The structural loads may potentially exacerbate subsidence caused by this process. Tidal flow and stormwater injection are candidates to explain the constant rate component of the observed subsidence.

6.4. How Long Will Subsidence Continue?

For exponential decaying subsidence, there is a potential that subsidence will eventually be arrested. However, for subsidence at constant rate there is no indication that subsidence will stop, in particular if subsidence is driven by tidal flow or stormwater injection. In both cases, nearby construction activities can act as a trigger to accelerate or re-accelerate the process of particle rearrangement, leading to additional subsidence through dynamic settlement.

Nevertheless, our current inability to fully comprehend the subsidence mechanism and the lack of comprehensive information on the underground strata, hinders our ability to predict the duration of the subsidence phenomenon.

6.5. Can Subsidence Cause Damages?

While South Florida high-rises are designed to undergo several tens of centimeters of settlement of the entire structure, differential settlement induces internal stresses that can lead to structural damage.

The differences in the averaged LOS velocities within the footprints of the Fendi and the Surf Club North structures by 0.2–0.3 cm/yr (1–2 cm over the study period, see Section 4.1.2) could be caused by differential settlement, tilting or rotations of the structures. Nevertheless, for exponentially decaying displacements the impacts will unlikely be significant. High-resolution SAR sensors such as TerraSAR-X and multiple viewing geometry are better suited for the detection of differential settlements compared to images from Sentinel-1 sensor because of a higher persistent scatterer density.

7. Conclusions

This study documents subsidence and settlement of coastal structures from Sunny Isles Beach to Miami Beach. Our conclusions are:

1. A total of 35 coastal buildings are undergoing subsidence of 2–8 cm in the vertical direction over the 2016–2023 period based on Sentinel-1 data. While TerraSAR-X data suggest over 10 cm of LOS displacement for Porsche Design Tower. Subsidence has linear to exponentially decaying characteristics and is most widespread in Sunny Isles Beach and Surfside while only a few structures are subsiding in Bal Harbor and Miami Beach. Sparse geological data suggest widespread sandy layers interbedded within the limestone of Sunny Isles Beach and less sandy layers further south. The limited geologic data suggest a correlation between subsidence and the amount of sandy layers in the limestone.
2. The majority of the subsiding buildings are new structures built after 2014. This suggests that subsidence is a consequence of their own construction. At older affected structures, the onset of subsidence mostly coincides with nearby construction activities.
3. Coherent pixels near subsiding buildings allow us to determine whether only the structures themselfs or also the surroundings are subsiding. Subsidence near the Surf Club in Surfside as well as subsidence of the older structures suggests that at these locations a broad sand layer is responsible for the subsidence. In contrast, we have identified four subsiding structures where only the structures themselves are subsiding (Oceana in Bal Harbor, 87 Park near Surfside, and L'Atelier and Faena House in Miami Beach).
4. We hypothesize that subsidence is primarily due to the gradual reconfiguration of the sand grains into a denser packing within sandy layers interbedded in the limestone. We further hypothesize that this grain rearrangement is instigated by construction activities, through either vibrations or groundwater flow in response to pumping during the initial construction phase (dynamic settlement). Another mechanism that could lead to grain rearrangement is the daily tidal flow through the sandy layers. Stormwater injection can also lead to subsidence by rearranging the sand grains or by dissolving the limestone. Overall, subsidence is likely caused by a combination of these mechanisms, with their specific contributions varying according to the local geological conditions.
5. There are no indications that subsidence will come to a stop. For structures subsiding at a constant rate this is obvious. For structures exhibiting a true exponential decay in subsidence, it could eventually cease. However, nearby construction vibrations are likely to restart the grain rearrangement process, leading to a renewed acceleration of subsidence.
6. Subsidence variability along the coast of Surfside highlights the influence of local geological conditions. While Champlain Towers South, the collapsed condominium, showed no subsidence of its rooftop despite significant vibrations from the adjacent 87 Park construction (which itself does exhibit settlement), subsidence of nearby low-rise buildings with relatively small structural loads (Cabarete and Residence Inn ~600 m north), is almost certainly driven by construction activities.
7. No measurement points are available for the section of the Champlain Towers South condominium where the collapse started because of the radar viewing geometry.

Data Availability Statement

The InSAR displacement results for Suuny Isles, Surfside and Bal Harbour, and Miami Beach are available on Zenodo (https://doi.org/10.5281/zenodo.12699617). Figures are prepared using GMT (Wessel et al., 2013) and Matplotlib (Hunter, 2007).

Acknowledgments
F.A., E.A. and F.A. acknowledge support from the University of Miami Laboratory For Integrative Knowledge (U-Link) Climate Resilience program. The work from P.M. and A.T. was performed at the University of Houston under a contract with the NASA Decadal Survey Incubation Program: Science and Technology (NNH21ZDA001N-DSI—80NSSC 22K1096). A. P. was supported by funding from the German Federal Ministry for Digital and Transport within the framework of SAR4Infra project. We thank Michael Sukop for suggesting tidal flow and stormwater injection as driving mechanisms and Randall Parkinson for discussions. The international collaboration was supported by a Helmholtz International Fellowship to FA. We thank Alfredo Tererro for help with data visualisation, Michael Sukop for suggesting tidal flowand storm water injection as driving mechanisms, Randall Parkinson for discussions, and Robert Zinke for his review. Sentinel-1 data were provided by the European Space Agency (ESA) through the Alaska European Space Agency (ESA) through the Alaska Satellite Facility (ASF) and TerraSAR-X data by the German Space Agency through project COA3837. For computations we used the Stampede3 system at Texas Advanced Computing Center (TACC) and Jetstream2 system at the Indiana University through allocation EAR200012 from the advanced Cyberinfrastructure Coordination Ecosystem: Services & Support (ACCESS) program, which is supported by U.S. National Science Foundation Grants 2138259, 2138286, 2138307, 2137603, and 2138296.

References

Amelung, F., Galloway, D. L., Bell, J. W., Zebker, H. A., & Laczniak, R. J. (1999). Sensing the ups and downs of las Vegas: InSAR reveals structural control of land subsidence and aquifer-system deformation. *Geology*, *27*(6), 483–486. https://doi.org/10.1130/0091-7613(1999)027<0483:stuado>2.3.co;2

Banks, K., Riegl, B., Shinn, E., Piller, W. E., & Dodge, R. E. (2007). Geomorphology of the Southeast Florida continental reef tract (Miami-Dade, Broward, and palm beach counties, USA). *Coral Reefs*, *26*(3), 617–633. https://doi.org/10.1007/s00338-007-0231-0

Bioucas-Dias, J. M., & Valadão, G. (2007). Phase unwrapping via graph cuts. *IEEE Transactions on Image Processing*, *16*(3), 698–709. https://doi.org/10.1109/tip.2006.888351

Boykov, Y., & Kolmogorov, V. (2004). An experimental comparison of min-cut/max-flow algorithms for energy minimization in vision. *IEEE Transactions on Pattern Analysis and Machine Intelligence*, *26*(9), 1124–1137. https://doi.org/10.1109/tpami.2004.60

Chaussard, E., Havazli, E., Fattahi, H., Cabral-Cano, E., & Solano-Rojas, D. (2021). Over a century of sinking in Mexico City: No hope for significant elevation and storage capacity recovery. *Journal of Geophysical Research: Solid Earth*, *126*(4), e2020JB020648. https://doi.org/10.1029/2020jb020648

Cunningham, K. J. (2004). Application of ground-penetrating radar, digital optical borehole images, and cores for characterization of porosity hydraulic conductivity and Paleokarst in the Biscayne aquifer, Southeastern Florida, USA. *Journal of Applied Geophysics*, *55*(1–2), 61–76. https://doi.org/10.1016/j.jappgeo.2003.06.005

Devanthéry, N., Crosetto, M., Monserrat, O., Cuevas-González, M., & Crippa, B. (2014). An approach to persistent scatterer interferometry. *Remote Sensing*, *6*(7), 6662–6679. https://doi.org/10.3390/rs6076662

Dörr, N., Schenk, A., & Hinz, S. (2022). On the relevance of temporary persistent scatterers for long-term Ps-InSAR monitoring. In *Eusar 2022; 14th European conference on synthetic aperture radar* (pp. 1–6).

Enos, P., & Perkins, R. (1977). *Quaternary sedimentation in south Florida*. Geological Society of America. Retrieved from https://books.google.com/books?id=uCFh2OGTtH0C

Evans, C. C. (1983). Depositional and diagenetic of Miami limestone. In *Proceedings from the symposium on South Florida geology*. Miami Geological Society. Miami, Fl.

Fiaschi, S., & Wdowinski, S. (2020). Local land subsidence in Miami Beach (Fl) and Norfolk (VA) and its contribution to flooding hazard in coastal communities along the us Atlantic coast. *Ocean & Coastal Management*, *187*, 105078. https://doi.org/10.1016/j.ocecoaman.2019.105078

Fish, J. E., & Stewart, M. T. (1991). Hydrogeology of the surficial aquifer system, Dade County, Florida. *US Department of the Interior, US Geological Survey*, *90*, 4108.

Henann, D. L., & Kamrin, K. (2014). Continuum modeling of secondary rheology in dense granular materials. *Physical Review Letters*, *113*(17), 178001. https://doi.org/10.1103/physrevlett.113.178001

Hoffmeister, J. E., Stockman, K., & Multer, H. G. (1967). Miami limestone of Florida and its recent Bahamian counterpart. *Geological Society of America Bulletin*, *78*(2), 175–190. https://doi.org/10.1130/0016-7606(1967)78[175:mlofai]2.0.co;2

Hunter, J. D. (2007). Matplotlib: A 2d graphics environment. *Computing in Science & Engineering*, *9*(3), 90–95. https://doi.org/10.1109/MCSE.2007.55

Kaderabek, T. J., & Reynolds, R. T. (1981). Miami limestone foundation design and construction. *Journal of the Geotechnical Engineering Division*, *107*(7), 859–872. https://doi.org/10.1061/ajgeb6.0001166

Kuwano, R., & Jardine, R. (2002). On the applicability of cross-anisotropic elasticity to granular materials at very small strains. *Géotechnique*, *52*(10), 727–749. https://doi.org/10.1680/geot.2002.52.10.727

Lade, P. V. (1994). Creep effects on static and cyclic instability of granular soils. *Journal of Geotechnical Engineering*, *120*(2), 404–419. https://doi.org/10.1061/(asce)0733-9410(1994)120:2(404)

Lade, P. V., & Liu, C.-T. (1998). Experimental study of drained creep behavior of sand. *Journal of Engineering Mechanics*, *124*(8), 912–920. https://doi.org/10.1061/(asce)0733-9399(1998)124:8(912)

Logan, L., & Singh, A. (2023). High-rise condominium collapse. *Journal of Legal Affairs and Dispute Resolution in Engineering and Construction*, *15*(1), 05022008. https://doi.org/10.1061/(asce)la.1943-4170.0000583

Ma, P., Lin, H., Wang, W., Yu, H., Chen, F., Jiang, L., et al. (2021). Toward fine surveillance: A review of multitemporal interferometric synthetic aperture radar for infrastructure health monitoring. *IEEE Geoscience and Remote Sensing Magazine*, *10*(1), 207–230. https://doi.org/10.1109/mgrs.2021.3098182

Massarsch, K. (2000). Settlements and damage caused by construction-induced vibrations. In *Proceedings of international workshop wave* (pp. 299–315).

Massarsch, K. R., & Fellenius, B. (2014). Ground vibrations from pile and sheet pile driving. Part 1 building damage. In *Proceedings of the international conference on piling and deep foundations* (pp. 131–139).

McDowell, G., & Khan, J. (2003). Creep of granular materials. *Granular Matter*, *5*(3), 115–120. https://doi.org/10.1007/s10035-003-0142-x

Mirzaee, S., Amelung, F., & Fattahi, H. (2023). Non-linear phase linking using joined distributed and persistent scatterers. *Computers & Geosciences*, *171*, 105291. https://doi.org/10.1016/j.cageo.2022.105291

Perissin, D., Wang, Z., & Wang, T. (2011). The sarproz InSAR tool for urban subsidence/manmade structure stability monitoring in China. *Proceedings of the ISRSE, Sidney*, *1015*.

Piter, A., Haghshenas Haghighi, M., Lab, F., & Motagh, M. (2024). Sarvey – Survey with SAR. *Zenodo*. https://doi.org/10.5281/zenodo.12544130

Piter, A., Haghshenas Haghighi, M., & Motagh, M. (2024). Challenges and opportunities of sentinel–1 InSAR for transport infrastructure monitoring. *Photogrammetrie, Fernerkundung, GeoInformation*, *92*(5), 609–627. https://doi.org/10.1007/s41064-024-00314-x

Saidi, K., TRE Altamira, Inc., & Exponent, Inc. (2024). *InSAR analysis over the eastern coastline of Florida* (Grant/Contract Reports). National Institute of Standards and Technology (NISTGCR). https://doi.org/10.6028/NIST.GCR.24-055

Scott, T. M. (2001). *Text to accompany the geologic map of Florida*. Florida Geological Survey.

Sobhan, K., & Reddy, D. V. (2015). *Damage to millennium condominium due to vibrations caused by the construction activities of the adjacent Porsche tower*. Geotechnical Consultant Report submitted to Milennium Condominium Board.

USGS. (2000). *GeoLog locator*. U.S. Geologicak Survey (USGS) public data domain. https://doi.org/10.5066/F7X63KT0

Wessel, P., Smith, W. H. F., Scharroo, R., Luis, J., & Wobbe, F. (2013). Generic mapping tools: Improved version released. *Eos, Transactions American Geophysical Union*, *94*(45), 409–410. https://doi.org/10.1002/2013EO450001

Yang, M., López-Dekker, P., Dheenathayalan, P., Biljecki, F., Liao, M., & Hanssen, R. F. (2019). Linking persistent scatterers to the built environment using ray tracing on urban models. *IEEE Transactions on Geoscience and Remote Sensing*, *57*(8), 5764–5776. https://doi.org/10.1109/TGRS.2019.2901904

Youd, T. L. (1977). Packing changes and liquefaction susceptibility. *Journal of the Geotechnical Engineering Division*, *103*(8), 918–922. https://doi.org/10.1061/ajgeb6.0000478

Zhao, F., & Mallorqui, J. J. (2019). A temporal phase coherence estimation algorithm and its application on Dinsar pixel selection. *IEEE Transactions on Geoscience and Remote Sensing*, *57*(11), 8350–8361. https://doi.org/10.1109/tgrs.2019.2920536

Erratum

The originally published version of this article contained typographical errors. All mentions of Section S1, Section S2, Section S3, and Section S4 of Supporting Information S1 should be changed to Section 1, Section 2, Section 3, and Section 4 of Supporting Information S1. The errors have been corrected, and this may be considered the authoritative version of record.